Eur. J. Mineral., 37, 733–746, 2025
https://doi.org/10.5194/ejm-37-733-2025

European Journal of Mineralogy
Open Access

Marioantofilliite, $[Cu_4Al_2(OH)_{12}](CO_3)\cdot 3H_2O$, a new member of the hydrotalcite supergroup from Liguria (Italy)

Cristian Biagioni[1,2], Jiří Sejkora[3], Natale Perchiazzi[1,2], Enrico Mugnaioli[1,2], Daniela Mauro[1,4], Donato Belmonte[5], Radek Škoda[6], and Zdeněk Dolníček[3]

[1]Dipartimento di Scienze della Terra, Università di Pisa, Via Santa Maria 53, 56126 Pisa, Italy
[2]Centro per l'Integrazione della Strumentazione scientifica dell'Università di Pisa (CISUP), Università di Pisa, 56126 Pisa, Italy
[3]Department of Mineralogy and Petrology, National Museum, Cirkusová 1740, 193 00 Prague 9, Czech Republic
[4]Museo di Storia Naturale, Università di Pisa, Via Roma 79, 56011 Calci (PI), Italy
[5]Dipartimento di Scienze della Terra, dell'Ambiente e della Vita (DISTAV), Università degli Studi di Genova, Corso Europa 26, 16132 Genova, Italy
[6]Department of Geological Sciences, Faculty of Science, Masaryk University, Kotlářská 2, 611 37, Brno, Czech Republic

Correspondence: Cristian Biagioni (cristian.biagioni@unipi.it)

Received: 16 May 2025 – Revised: 23 June 2025 – Accepted: 30 July 2025 – Published: 14 October 2025

Abstract. Marioantofilliite (IMA 2025-012), ideally $[Cu_4Al_2(OH)_{12}](CO_3)\cdot 3H_2O$, is a new member of the hydrotalcite supergroup discovered in the Cu–Fe ore deposit of Monte Copello–Reppia, Graveglia Valley, Liguria, Italy. It occurs as globular aggregates up to 1 mm in diameter formed by µm-sized prismatic crystals. The streak is light blue, and lustre is greasy. Calculated density is 2.825 g cm^{-3}. Marioantofilliite is optically biaxial (–), with $\alpha = 1.613(4)$, $\beta = 1.626(3)$, and $\gamma = 1.633(5)$ (in 589 nm light). $2V_{calc}$ is 72°. It is distinctly pleochroic, ranging from colourless to pale blue. The empirical chemical formula of marioantofilliite (with rounding errors) is $[Cu^{2+}_{4.23}Mg_{0.02}Al_{1.76}(OH)_{12}](CO_3)_{0.82}(SO_4)_{0.01}[Si(OH)_6]_{0.05}\cdot 3H_2O$. Unit-cell parameters of marioantofilliite are $a = 5.590(3)$, $b = 2.9358(11)$, $c = 7.675(3)$ Å, $\beta = 100.958(17)°$, and $V = 123.66(9)$ Å^3, with space group $C2/m$ and $Z = 1/3$. The crystal structure was refined to $R_1 = 0.0372$ for 181 unique reflections with $F > 4\sigma(F)$ and 23 refined parameters. It is topologically similar to that of other hydrotalcite-supergroup minerals and shows a distorted {001} brucite-like layer with Cu and Al statistically occupying an octahedrally coordinated $M(1)$ site. The interlayer hosts disordered CO_3 and H_2O groups. Marioantofilliite formed through the oxidative dissolution of primary Cu ores by mine drainage aqueous solutions and neutralization by gangue carbonates. Its name honours Mario Antofilli (1920–1983) for his contributions to the knowledge of the mineralogy of Liguria.

1 Introduction

Jurassic ophiolitic rocks cropping out in the northern Apennines (Italy) host several volcanogenic massive sulfide Cu(–Zn) ore deposits that were exploited up to the first half of the 20th century (e.g. Ferrario and Garuti, 1980; Garuti et al., 2008; Dini et al., 2024). Few modern mineralogical studies are currently available on primary ore minerals (e.g. Bertolani and Rivalenti, 1973), even if Dini et al. (2024) highlighted the local occurrence of (Te–Se–Ag–Au–Pb)-bearing mineral assemblages. Among gangue minerals, some ore deposits are characterized by the presence of zeolites, for instance in the Montecatini Val di Cecina mine (Tuscany), where several new zeolite species were described during the 19th century (e.g. D'Achiardi, 1873) and were later discred-

ited due to being identical to previously known species (e.g. Franzini and Perchiazzi, 1994). The only zeolite having its type locality in this kind of occurrence is heulandite-Sr from the Campegli mine (Castiglione Chiavarese, Genoa Province, Liguria), first reported by Lucchetti et al. (1982) and later approved as a valid mineral species by Coombs et al. (1997). Secondary mineral assemblages have not been the focus of detailed mineralogical investigations so far, even if in some cases some information was published by mineral collectors (e.g. Camarda et al., 2013; Bardi et al., 2017). Only recently, following these studies, was the first new supergene mineral species related to the alteration of ophiolite-hosted Cu ore deposits, i.e. tiberiobardiite, discovered (Biagioni et al., 2018).

During the examination of some supergene minerals from the Monte Copello–Reppia Cu prospect, in the Graveglia Valley, Genoa Province, Liguria (Italy), a phase dubiously identified as carbonatecyanotrichite was provided by the mineral collector Sebastiano Di Lisi. Examination through X-ray powder diffraction clearly indicated that the studied sample was the natural analogue of some synthetic "Cu–Al hydrotalcite" (hereafter Cu–Al layered double hydroxide, Cu–Al LDH) phases (e.g. Yamaoka et al., 1989; Britto and Kamath, 2009). Further investigations allowed us to confirm the preliminary data and to fully characterize this new mineral species, which was named marioantofilliite. The new mineral, its name, and its symbol (Maf) have been approved by the IMA Commission on New Minerals, Nomenclature and Classification (proposal IMA # 2025-012). The name honours Mario Antofilli (1920–1983) for his contribution to the knowledge of the mineralogy of Liguria. During the 1970s and up to his death, he was active in supporting the activities of the *Gruppo Mineralogico Ligure*, where he served as president for many years. Mario Antofilli was author, along with Emilio Borgo and Andrea Palenzona, of the book *I nostri minerali – Geologia e Mineralogia in Liguria*, printed in 1983 (Antofilli et al., 1983). Moreover, he published a comprehensive review on Ligurian zeolites (Antofilli, 1982). His findings at the Molinello mine (Graveglia Valley) in the mid-1970s allowed the discovery of tiragalloite, the first natural arsenatotrisilicate (Gramaccioli et al., 1980). Type material of marioantofilliite is represented by two cotype specimens. One specimen (oxidized ore sample and single crystal used for X-ray diffraction study) is kept in the mineralogical collection of the Museo di Storia Naturale of the University of Pisa, Via Roma 79, Calci (Pisa, Italy), under catalogue number 20081. The other specimen (polished grain used for WDS chemical analysis) is kept in the National Museum, Prague, under catalogue number P1P 3/2025.

2 Occurrence and physical properties

Marioantofilliite was discovered in the mining prospect of Monte Copello–Reppia (latitude 44°23′11.40″ N, longitude 9°27′25.17″ E), Graveglia Valley, Ne, Genoa Province, Liguria, Italy.

The Cu–Fe ore deposit formerly exploited at Monte Copello belongs to a series of small ore bodies occurring around Reppia and described by several authors (Bonatti and Trevisan, 1941; Ferrario and Garuti, 1980; Garuti et al., 2008; Alt et al., 2018). These ore bodies are stratiform and are located at the contact between serpentinite and pillow basalts (Type 1 of Garuti et al., 2008) or at the interface between brecciated basalts and the sedimentary cover represented by cherts (Diaspri di Monte Alpe Fm) and Calpionella limestone (Type 2 of Garuti et al., 2008); finally, stockwork veins protrude from the stratiform Type 2 ore bodies downward within the brecciated basalts. The Monte Copello prospect exploited a sulfide ore body, mainly represented by pyrite and chalcopyrite within a gangue of calcite, quartz, and clay minerals, at the tectonized contact between basalts and Calpionella limestone. The ore body is deeply weathered, and it is represented by gossan. Several supergene phases have been observed within its vugs. Camarda et al. (2013) described the following species: allophane, brochantite, carbonatecyanotrichite, connellite, chrysocolla, cuprite, delafossite, felsőbányaite (?), gypsum, langite, malachite, and native copper.

Marioantofilliite occurs as globular aggregates, up to 1 mm in diameter, sometimes showing µm-sized prismatic crystals of marioantofilliite (Fig. 1). The colour is blue, and the streak is light blue. Lustre is greasy. The mineral is transparent, and it does not fluoresce under short- and long-wavelength UV radiation. Marioantofilliite is soft and brittle. Cleavage and fracture were not observed owing to the very small crystal size. Calculated density is 2.825 g cm^{-3} based on the empirical formula and unit-cell parameters measured using single-crystal X-ray diffraction. Marioantofilliite is transparent. It is biaxial (–), with $\alpha = 1.613(4)$, $\beta = 1.626(3)$, and $\gamma = 1.633(5)$ (determined in 589 nm light). The $2V$ angle calculated by ExcalibrW software from the extinction on the spindle stage is 69°, whereas the calculated $2V$ value based on the refraction indices using the equation of Wright (1951) is 72°. Dispersion is strong, with $r > v$. Marioantofilliite is distinctly pleochroic, with X = colourless and Z = pale blue. The optical orientation could not be determined because of the poor quality of the examined material. The compatibility index $[1 - (K_P/K_C)]$ is 0.006, within the "superior" range (Mandarino, 1981).

In type material, marioantofilliite is associated with allophane and malachite on limonite (Fig. 1). Its genesis is related to the oxidative dissolution of the primary Cu ores by mine drainage aqueous solutions and neutralization by gangue carbonates (e.g. Majzlan et al., 2018). According to Yamaoka et al. (1989), Cu–Al LDH can be stable in circumneutral pH conditions (i.e. pH range 6–8) at ambient conditions.

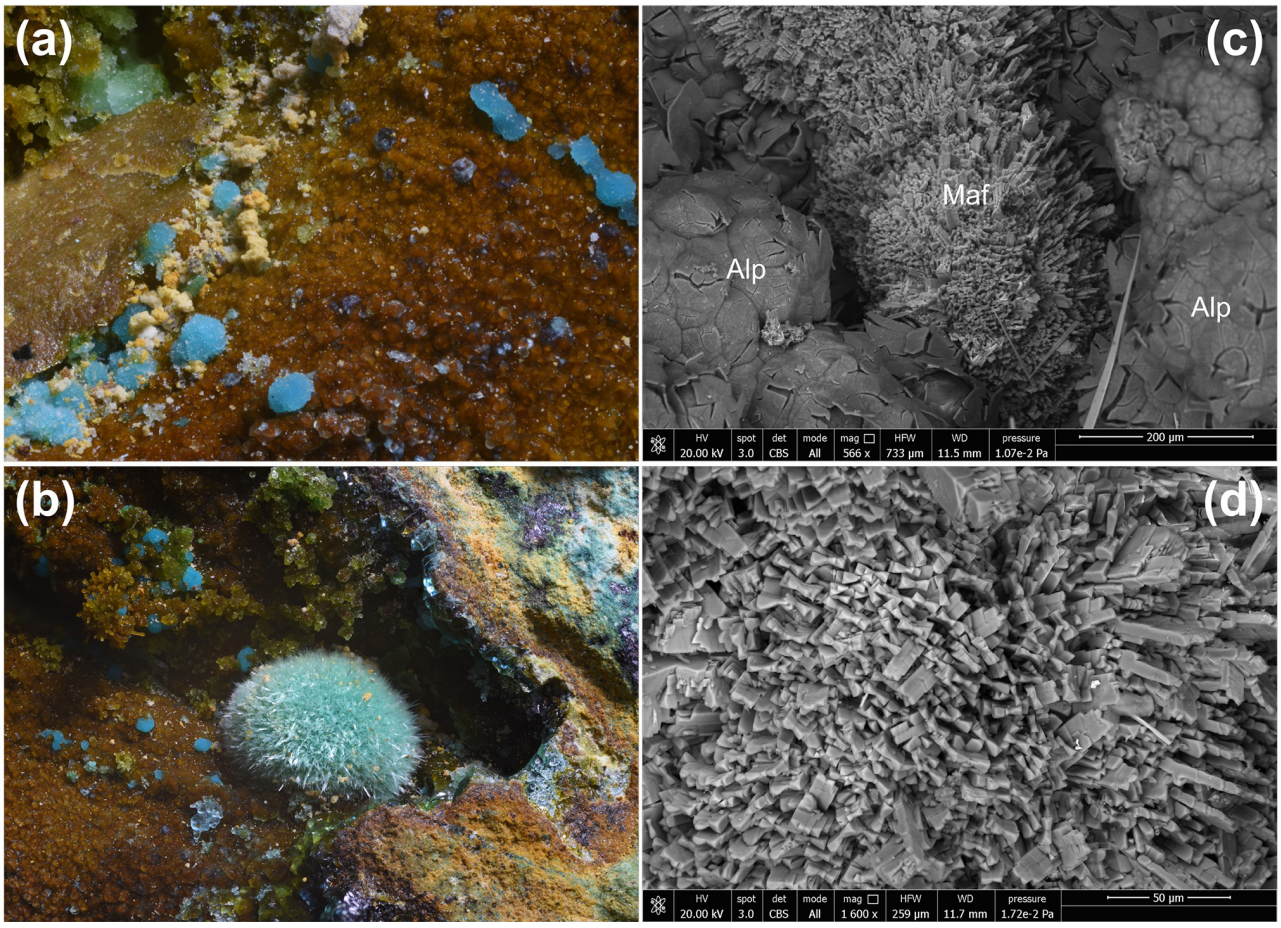

Figure 1. Marioantofilliite, as blue globular aggregates on allophane **(a)**, in some cases associated with greenish crystalline globular aggregates of malachite **(b)**. The SEM pictures show the morphology of marioantofilliite aggregates **(c)** and crystals **(d)**. Symbols: Alp is allophane; Maf is marioantofilliite. Monte Copello–Reppia, Graveglia Valley, Ne, Genoa Province, Liguria, Italy. Type material, Natural History Museum of the University of Pisa.

3 Raman spectroscopy

The Raman spectrum of marioantofilliite was collected in the range of 4000–20 cm^{-1} using a DXR dispersive Raman spectrometer (Thermo Scientific) mounted on a confocal Olympus microscope (National Museum, Prague). The Raman signal was excited by an unpolarized green diode-pumped solid-state laser ($\lambda = 532$ nm) and detected by a CCD detector. The experimental parameters were 100× objective, 10 s exposure time, 100 exposures, 400 lines mm^{-1} grating, 50 µm slit spectrograph aperture, and 5 mW laser power level. The thermal damage of the measured points was excluded by the visual inspection of the excited surface after measurement, by the observation of the possible decay of spectral features in the start of excitation, and by checking for the thermal downshift of Raman lines. The instrument was set up by a software-controlled calibration procedure using multiple Ne emission lines (wavelength calibration), multiple polystyrene Raman bands (laser frequency calibration), and standardized white-light sources (intensity calibration). Spectral manipulations were performed using the Omnic 9 software (Thermo Scientific).

The Raman spectrum of marioantofilliite in the full range is given in Fig. 2. Its interpretation is based on the papers by Pérez-Ramírez et al. (2001), Frost et al. (2009), Vieira et al. (2009), Čejka et al. (2013), Theiss et al. (2015), and Zhitova et al. (2024) and references therein. The strongest band at 3520 cm^{-1}, with a shoulder at 2935 cm^{-1}, is assigned to the ν O–H stretching vibrations of the hydrogen-bonded OH and H_2O groups. The very weak bands at 1659 and 1395 cm^{-1} are attributed to the ν_2 (δ) bending vibrations of H_2O groups and the doubly degenerate ν_3 CO_3^{2-} antisymmetric stretching vibrations, respectively. A medium strong band at 1060 cm^{-1} relates to the ν_1 CO_3^{2-} symmetric stretching vibrations. Bands related to the ν_2 (δ) CO_3^{2-} out-of-plane bending (about 880 cm^{-1}) and doubly degenerate ν_4 (δ) CO_3^{2-} in-plane bending (about 680 cm^{-1}) vibrations were not observed in the experimental spectrum. A strong

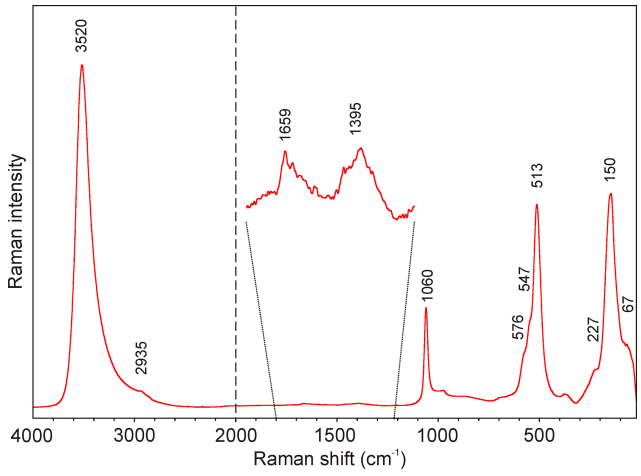

Figure 2. Raman spectrum of marioantofilliite in the full range (4000–20 cm^{-1}, split at 2000 cm^{-1}).

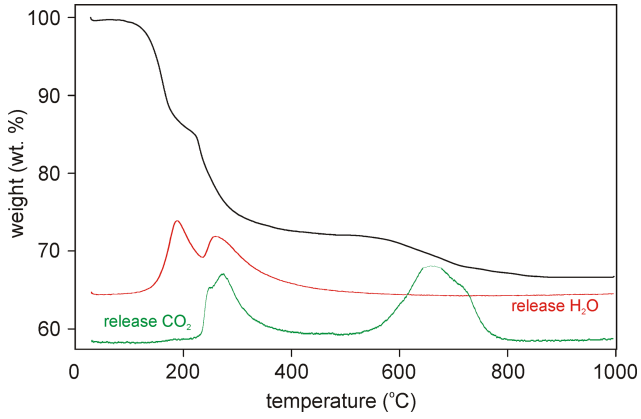

Figure 3. Thermogravimetric curve (black) for marioantofilliite. Red and green lines show the release of H_2O and CO_2, respectively, as a function of temperature.

band at 513 cm^{-1} with shoulders at 576 and 547 cm^{-1} can be assigned to the M–O symmetric stretching, and a band at 150 cm^{-1}, with a shoulder at 227 cm^{-1}, can be assigned to the O–M–O bending vibrations, whereas the weak band at 67 cm^{-1} is due to the lattice mode.

4 Thermogravimetric and evolved-gas analyses

Thermogravimetric and evolved-gas data on marioantofilliite were collected at the University of Chemistry and Technology (Prague, Czech Republic) using a Thermobalance SETSYS (Setaram, France) equipped with a mass spectrometer, GSD 320 03 OmniStar (Pfeiffer Vacuum, Austria). The sample weighing 1.316 mg was analysed between 30 and 995 °C in air (20 mL min^{-1}) with a heating rate 10 °C min^{-1}. The collected thermogravimetric curve is shown in Fig. 3. Four main weight loss steps can be identified, in accord with Boulahbal et al. (2023): (i) between 30 and 230 °C, (ii) between 230 and 550 °C, (iii) between 550 and 780 °C, and (iv) between 780 and 995 °C. The first step (16.43 wt %) corresponds to the loss of ca. 3 H_2O and 5.5 (OH) groups. The second weight loss (11.81 wt %) is connected to dominant dehydration (ca. 9.35 wt % ∼ 6.5 (OH) groups) and the loss of a small fraction of CO_2 (ca. 2.46 wt % ∼ 0.35 CO_2). The simultaneous loss of both chemical constituents is documented by mass spectrometry. The third step of weight loss (4.44 wt %) corresponds to the full decomposition of CO_3 units (∼ 0.63 CO_2 molecules). Finally, the fourth step (0.59 wt %) is probably connected with formation of the reaction end-products tenorite (CuO) and $CuAl_2O_4$ spinel (O'Neill et al., 2005), which were identified by powder X-ray diffraction. The total observed weight loss, 33.27 wt % in the range 30–995 °C, is comparable with the ideal $H_2O + CO_2$ contents in marioantofilliite, i.e. 33.62 wt % (31.86 wt % in the normalized analysis), assuming 3 H_2O groups per formula unit as in other quintinite-group minerals. The small difference between these values is most likely caused by the minor admixture of other mineral phases in the measured sample or some analytical uncertainties.

5 Chemical data

Quantitative chemical analyses of marioantofilliite were carried out using a Cameca SX 100 electron microprobe (WDS mode, 15 kV, 10 nA, 5 µm beam diameter) on a polished surface at the National Museum, Prague, Czech Republic. Results (average of 20 spot analyses) are given in Table 1. Other sought elements (As, Na, P, Ca, Mn, Ba, Pb, Sr, Fe, Ni, Co, and Zn) were below detection limits. Matrix correction by the PAP algorithm (Pouchou and Pichoir, 1985) was applied to the data. The occurrence of CO_3 and H_2O groups was confirmed by micro-Raman spectroscopy and TG analysis coupled with mass spectrometry. Moreover, marioantofilliite rapidly dissolves in cold ∼ 3.3 M HCl with a strong effervescence, further confirming the presence of CO_3 groups. As not enough pure material was available for a direct determination of H_2O, the latter was calculated based upon the assumed stoichiometry.

The general layer formula of hydrotalcite-supergroup minerals can be written as $[M^{2+}_{1-x}M^{3+}_{x}(OH)_2]^{x+}$ (Mills et al., 2012a). In the studied specimen, $x \sim 0.29$, resulting in the layer composition $[(Cu,Mg)_{0.71}Al_{0.29}(OH)_2]^{0.29+}$. The ratio between M^{2+} and M^{3+} cations is ∼ 2.45, intermediate between the ratio of members of the quintinite group ($M^{2+} : M^{3+} = 2$) and the hydrotalcite group ($M^{2+} : M^{3+} = 3$). According to the observed basal spacing, i.e. ∼ 7.6 Å, marioantofilliite probably belongs to the quintinite group, in accord with Zhitova et al. (2016). It is worth noting that deviations from the ideal $M^{2+} : M^{3+}$ ratio of 2 : 1 are known in this group. For instance, Zhitova et al. (2016) reported ratios of up to 2.38, not far from the value observed in marioantofil-

Table 1. Chemical data (in wt %) for marioantofilliite.

Constituent	Average ($n = 20$)	Range	e.s.d. (σ)	Normalized	Standard
SO_3	0.07	0.00–0.16	0.04	0.07	celestine
CO_{2calc}	6.06			5.74	
SiO_2	0.54	0.04–1.61	0.40	0.51	wollastonite
Al_2O_3	14.97	14.20–16.01	0.51	14.19	sanidine
MgO	0.12	0.00–0.31	0.12	0.11	diopside
CuO	56.21	53.54–60.20	1.93	53.26	chalcopyrite
H_2O_{calc}	27.56			26.12	
Total	105.53			100.00	

Note: H_2O and CO_2 contents were based on stoichiometry; e.s.d.: estimated standard deviation; n: number of spot analyses.

liite. Moreover, as shown by synthesis experiments, a series between $x = 0.14$ and $x = 0.50$ seems to occur (Yamaoka et al., 1989); for instance, Intissar et al. (2015) obtained a phase with $x = 0.33$ and layer composition $[Cu_4Al_2(OH)_{12}]^{2+}$. In accord with the observed x value and the results of Zhitova et al. (2016), this latter layer composition is assumed for marioantofilliite.

The empirical formula of marioantofilliite was thus calculated on the basis of $(Cu + Mg + Al) = 6$ atoms per formula unit (apfu), assuming an amount of $(CO_3)^{2-}$ in accord with the electrostatic balance, considering also the occurrence of $(SO_4)^{2-}$ and $[Si(OH)_6]^{2-}$. The occurrence of interstitial $[Si(OH)_6]^{2-}$ groups was proposed by some authors, e.g. Kolitsch et al. (2013). However, it is probable that minor SO_3 and SiO_2 are due to some admixed phase(s). With respect to the ideal $M^{2+} : M^{3+}$ ratio of 4 : 2, the ratio of $(Cu + Mg) : Al$ is 4.25 : 1.76. This suggests that there should be some mechanism decreasing the interlayer negative charge, e.g. $M^{3+} + (CO_3, SO_4, [Si(OH)_6])^{2-}_{0.5} = M^{2+} + \square$. The empirical formula of marioantofilliite can thus be written (with rounding errors) as $[Cu^{2+}_{4.23}Mg_{0.02}Al_{1.76}(OH)_{12}](CO_3)_{0.82}(SO_4)_{0.01}[Si(OH)_6]_{0.05} \cdot 3H_2O$. The end-member formula is $[Cu_4Al_2(OH)_{12}](CO_3) \cdot 3H_2O$, corresponding to (in wt %) CO_2 7.03, Al_2O_3 16.28, CuO 50.80, and H_2O 25.89, sum 100.00.

6 Crystallography

6.1 Powder X-ray diffraction

Powder X-ray diffraction data of marioantofilliite (available in the Supplement) were collected using a Bruker D8 Venture single-crystal diffractometer equipped with a Photon III CCD area detector (microfocus Cu$K\alpha$ radiation) simulating a Gandolfi-like geometry (CISUP, University of Pisa, Italy). The observed X-ray diffraction lines are reported in Table 2, along with the calculated pattern based on the structural model discussed below. Unit-cell parameters were refined using the software Topas-Academic (Coelho, 2018) and are as follows: $a = 5.5815(6)$, $b = 2.9374(4)$, $c = 7.6878(9)$ Å, $\beta = 100.925(9)°$, and $V = 123.76(2)$ Å^3, with space group $C2/m$.

6.2 Single-crystal X-ray diffraction

Single-crystal X-ray diffraction intensity data were collected using a Bruker D8 Venture single-crystal diffractometer equipped with an air-cooled Photon III CCD detector and microfocus Mo$K\alpha$ radiation (CISUP, University of Pisa, Italy). The detector-to-crystal distance was 38 mm. Data were collected using ω and φ scan modes, in 0.5° slices, with an exposure time of 30 s per frame. A total of 2220 frames were collected. The frames were integrated with the Bruker SAINT software package using a narrow-frame algorithm. Data were corrected for Lorentz polarization, absorption, and background using the Apex4 software package (Bruker AXS Inc., 2022). Unit-cell parameters, refined on the basis of the XYZ centroid of 801 reflections above $20\sigma(I)$ with $5.406° < 2\theta < 58.21°$, are $a = 5.590(3)$, $b = 2.9358(11)$, $c = 7.675(3)$ Å, $\beta = 100.958(17)°$, and $V = 123.66(9)$ Å^3. The statistical tests on the distribution of $|E|$ values ($|E^2 - 1| = 0.495$) do not clearly indicate the occurrence of a centre of symmetry. According to the systematic absences and the uncertainty about the occurrence of a centre of symmetry, the crystal structure of marioantofilliite was solved in three different space groups using *Shelxtl* (Sheldrick, 2015a), i.e. $C2/m$, $C2$, and Cm. The main structural features are very similar in these three models. However, the $C2$ and Cm structural models gave racemic twin ratios close to 0.5, suggesting the presence of a centre of symmetry. For this reason, the crystal structure of marioantofilliite was refined, using *Shelxl*-2018 (Sheldrick, 2015b) in the space group $C2/m$. Neutral scattering curves, taken from the *International Tables for Crystallography* (Wilson, 1992), were used. In the first stage of the refinement, a slightly distorted brucite-like layer formed by (Cu,Al)-centred octahedra was found. The occupancy of the $M(1)$ site was refined

Table 2. X-ray powder diffraction data (d in Å) for marioantofilliite compared with those of synthetic Cu–Al LDH phases.

Marioantofilliite					PDF 46-099 (Yamaoka et al., 1989)			Britto and Kamath (2009)	
I_{obs}	d_{obs}	d_{calc}	I_{calc}	hkl	d_{hkl}	I_{hkl}	hkl	d_{hkl}	hkl
100	7.56	7.54	100	0 0 1	7.538	100	0 0 2	7.481	0 0 2
0.1	5.54	–	–	–	–	–	–	–	–
0.1	4.91	–	–	–	–	–	–	–	–
26	3.778	3.768	27	0 0 2	3.764	36	0 0 4	3.741	0 0 4
0.1	3.406	–	–	–	–	–	–	–	–
0.2	2.889	–	–	–	–	–	–	–	–
5	2.750	2.752	2	−2 0 1	2.727	11	2 0 −3	2.741	2 0 1
		2.744	12	2 0 0					
0.5	2.594	2.589	1	1 1 0	2.592	3	1 1 0		
8	2.524	2.519	15	−1 1 1	2.515	15	−1 1 2	2.519	1 1 1
4	2.438	2.451	1	−2 0 2	2.416	2	1 1 2	–	–
		2.434	10	2 0 1					
1.5	2.388	2.383	3	1 1 1	2.380	1	−1 1 3	2.389	1 1 2
7.5	2.233	2.229	12	−1 1 2	2.230	9	1 1 3	2.227	1 1 3
0.1	2.140	–	–	–	–	–	–	–	–
		2.058	1	−2 0 3					
3.9	2.044	2.050	2	1 1 2	–	–	–	2.039	2 1 −2
		2.041	7	2 0 2					
0.1	1.958	–	–	–	–	–	–	–	–
8.2	1.892	1.889	11	−1 1 3	–	–	–	1.891	0 1 6
		1.884	1	0 0 4					
0.1	1.805	–	–	–	–	–	–	–	–
2.4	1.731	1.727	5	1 1 3	–	–	–		
2.6	1.728	1.712	2	−2 0 4	1.718	3	2 0 −8	1.721	0 1 7
0.8	1.702	1.699	2	2 0 3	–	–	–	–	–
1.8	1.595	1.593	3	−1 1 4	1.597	2	−3 1 3	1.587	1 1 7
1.2	1.573	1.572	5	−3 1 1	1.569	3	3 1 1	1.568	3 1 1
0.7	1.554	1.553	3	3 1 0				1.559	3 1 −4
0.9	1.526	1.525	3	−3 1 2	1.522	1	3 1 2	1.521	3 1 2
		1.474	1	3 1 1					
1.4	1.467	1.468	2	0 2 0	1.469	2	1 1 8	1.465	4 0 −2
		1.462	2	1 1 4					
1.5	1.443	1.442	1	−2 0 5	1.444	2	0 2 1	1.442	4 0 0
		1.441	2	0 2 1					

I_{calc} and d_{calc} were obtained using *PowderCell* 2.4 (Kraus and Nolze, 1996) on the basis of the structural model of marioantofilliite given in Table 4. Only calculated reflections with $I_{calc} > 1$ are reported.

using the scattering curves of Cu vs. Al. Some partially occupied sites occurred in the interlayer, and they were interpreted as *C* and O sites. The site occupancy of the *C* site was constrained to be half the occupancy of Al, in accord with the substitution $2Cu^{2+} + \square = 2Al^{3+} + (CO_3)^{2-}$. The two partially occupied positions interpreted as O-bearing sites are ca. 1.3 Å from the *C* site. However, whereas the site occupancy at the O($2i$) (i stands for interstitial) site was constrained to be the same as that of the *C* site, the site occupancy at O($1i$) was freely refined. Indeed, O($1i$) could be occupied by an O atom belonging to a CO_3 group or to an H_2O group. Finally, a maximum residual at ca. 1 Å from the O site coordinating (Cu,Al) atoms was found and interpreted as an H atom. The atoms of the brucite-like layer were refined anisotropically, whereas the H atom and interlayer partially occupied atom positions (for C and O) were refined isotropically. After several cycles of refinement, the conventional R factor converged to 0.0372 for 181 unique reflections with $F > 4\sigma(F)$ and 23 refined parameters. Details of the data collection and crystal structure refinement are given in Table 3. Atom coordinates and isotropic or equivalent isotropic displacement parameters are reported in Table 4, whereas Table 5 gives selected bond distances. Bond-valence calculation, shown in Table 6, was performed using the bond parameters of Gagné and Hawthorne (2015).

Table 3. Crystal and experimental data for marioantofilliite.

Crystal data	
Crystal size (mm)	$0.035 \times 0.006 \times 0.006$
Cell setting, space group	Monoclinic, $C2/m$
a (Å)	5.590(3)
b (Å)	2.9358(11)
c (Å)	7.675(3)
β (°)	100.958(17)
V (Å^3)	123.66(9)
Z	1/3
Data collection and refinement	
Radiation, wavelength (Å)	Mo$K\alpha$, 0.71073
Temperature (K)	299(2)
$2\theta_{max}$ (°)	56.38
Measured reflections	1682
Unique reflections	182
Reflections with $F > 4\sigma(F)$	181
R_{int}	0.0640
$R\sigma$	0.0325
Range of h, k, l	$-7 \le h \le 7$, $-3 \le k \le 3$, $-10 \le l \le 10$
$R[F > 4\sigma(F)]$	0.0372
R (all data)	0.0372
wR (on F^2)	0.0893
Goodness of fit	1.141
Number of least-squares parameters	23
Maximum and minimum residual peak (e Å^{-3})	0.78 (at 0.97 Å from $M(1)$) -0.68 (at 0.97 Å from $M(1)$)

Table 4. Sites, Wyckoff positions, site occupancy (s.o.), fractional atomic coordinates, and isotropic (*) or equivalent isotropic displacement parameters (in Å^2) for marioantofilliite.

Site	Wyckoff position	s.o.	x/a	y/b	z/c	$U_{eq/iso*}$
$M(1)$	$2b$	$Cu_{0.613(18)}Al_{0.387(18)}$	0	1/2	0	0.0160(4)
O(1)	$4i$	$O_{1.00}$	0.1079(9)	0	0.8682(5)	0.0334(14)
H	$4i$	$H_{1.00}$	0.072(15)	0	0.743(3)	0.050*
C	$4i$	$C_{0.097(5)}$	0.330(11)	0	0.492(8)	0.029(12)*
O($1i$)	$4i$	$O_{0.34(3)}$	0.104(5)	0	0.501(3)	0.069(8)*
O($2i$)	$4g$	$O_{0.193(9)}$	0	0.830(15)	1/2	0.064(10)*

6.3 Looking for a possible superstructure

The crystal structure of marioantofilliite solved and refined using single-crystal X-ray diffraction data is an average structure, as indicated by the disorder affecting the interlayer constituents. Although no superstructure reflections were observed during single-crystal X-ray diffraction experiments, very weak and unindexed reflections occurring in the X-ray powder diffraction pattern (Table 2) are probably associated with the occurrence of a superstructure.

In order to look for superstructure reflections, electron three-dimensional diffraction data (3DED) (e.g. Gemmi et al., 2019) were collected using a JEOL JEM-F200 Multipurpose TEM, operating at 200 kV and equipped with a Schottky field emission gun (FEG) source and an ASI CheeTah hybrid single-electron detector (516×516 pixels, 24 bit) (CISUP, University of Pisa, Italy). The 3DED dataset was acquired in STEM mode with a low-dose pseudo-parallel electron beam of about 30 nm of diameter, obtained through a 10 µm condenser aperture and a designated lens configuration. The diffraction quality of the examined grains was bad, possibly because the structure got damaged by the TEM vacuum, and only a pseudo-hexagonal cell was suggested. It is notewor-

Table 5. Selected bond distances (in Å) and angles (°) for marioantofilliite.

$M(1)$	–O(1) ×4	1.942(3)	C	–O(1i)	1.28(6)
	–O(1) ×2	2.233(5)		–O(2i) × 2	1.35(5)
	average	2.039		average	1.33
	O–H	H···O	O···O	O–H···O angle	
O1–H···O(1i)	0.94(2)	1.90(4)	2.81(2)	163(7)	
O1–H···O(1i)	0.94(2)	1.95(4)	2.86(2)	162(8)	
O1–H···O(2i)	0.94(2)	1.90(2)	2.820(9)	164.8(13)	

Table 6. Bond-valence balance (in valence units, v.u.) for marioantofilliite.

	O(1)	O(1i)	O(2i)	$\Sigma_{cations}$	Expected
$M(1)$	$^{4\times\rightarrow}0.48^{\downarrow\times2}$			2.34	2.39
	$^{2\times\rightarrow}0.21$				
C		1.34	$^{2\times\rightarrow}1.13$	3.60	4.00
Σ_{anion}	1.17	1.34[a]	1.13[a]		
H bond	−0.16[b]	+0.18	+0.18		
	−0.18[c]	+0.16	+0.18		
Σ'_{anions}	0.99[b]	1.68	1.49		
	1.01[c]				

Left and right superscripts refer to bonds involving anions and cations, respectively. [a] Applies when the C site is occupied. [b] Applies when the O···O distance is 2.81 Å. [c] Applies when the O···O distance is 2.86 Å. Σ'_{anions} represents bond-valence sums corrected for H bonds, with values calculated following the method of Ferraris and Ivaldi (1988).

thy that the two unit-cell parameters of the brucite-like layer are different and close to the values 3.0 × 3.2 Å, with a γ angle close to 120°. The third parameter could not be obtained due to intense diffuse scattering in this direction. The two values measured experimentally are consistent with the $a = 2.94$, $b = 3.15$ Å, and $\gamma = 117.7°$ of the Niggli-reduced cell of marioantofilliite, obtained through the transformation matrix [0 −1 0 |1/2 1/2 0| 0 0 1]. Owing to the bad crystal quality, no electron diffraction intensity useful for a crystal structure refinement could be integrated.

7 Crystal structure

7.1 General structural features

The crystal structure of marioantofilliite (Fig. 4) is topologically similar to that of other hydrotalcite-supergroup minerals. It shows a distorted {001} brucite-like layer, with Cu and Al statistically occupying an octahedrally coordinated $M(1)$ site. In the interlayer, three atom positions have been located. One was modelled as occupied by C atoms, whereas the other positions were assumed to be occupied by O atoms. Short C–C and O–O distances indicate the necessity of a short-range order of the partially occupied positions.

7.2 Cation coordination

Copper and aluminium statistically occupy the $M(1)$ site. This position shows a distorted (4 + 2) octahedral coordination, with four equatorial bonds at 1.94 Å and two apical ones at 2.23 Å. This geometry is probably due to the Jahn–Teller effect of Cu^{2+} (Burns and Hawthorne, 1996). The refined site occupancy is $Cu_{0.613(18)}Al_{0.387(18)}$, to be compared with a theoretical value close to $Cu_{0.70}Al_{0.30}$ derived from chemical data. The bond-valence sum, calculated using the refined site occupancy, is 2.34 valence units (v.u.), compared to 2.39 v.u. expected from the refined site occupancy. Such a bond-valence sum value would be close to the ideal occupancy $Cu_{0.67}Al_{0.33}$. In every case, the observed value is in accord with a mixed (Cu,Al) occupancy at the $M(1)$ site.

Carbon atoms are hosted at the C site. Every C atom is at too short a distance from other three C atoms. Two of them are at 1.74(6) Å, whereas the third is at 1.88(12) Å. This indicates that an ordered distribution of C atoms should occur in the interlayer. Moreover, there are C–O distances agreeing with those observed in CO_3 groups, i.e. C–O(1i) 1.28(6) Å and two C–O(2i) distances at 1.35(5) Å. Other C–O distances at 1.512(16) and 1.93(6) Å are interpreted as due to the disorder affecting the interlayer. The O–C–O angles, which in ideal CO_3 groups are 120°, range between 92(5) and 134(2)°. The bond-valence sum at the C atom is 3.60 v.u., lower than the ideal value of 4 v.u.; however, this value suffers from the uncertainty in the accurate determination of the atom position of interlayer atoms.

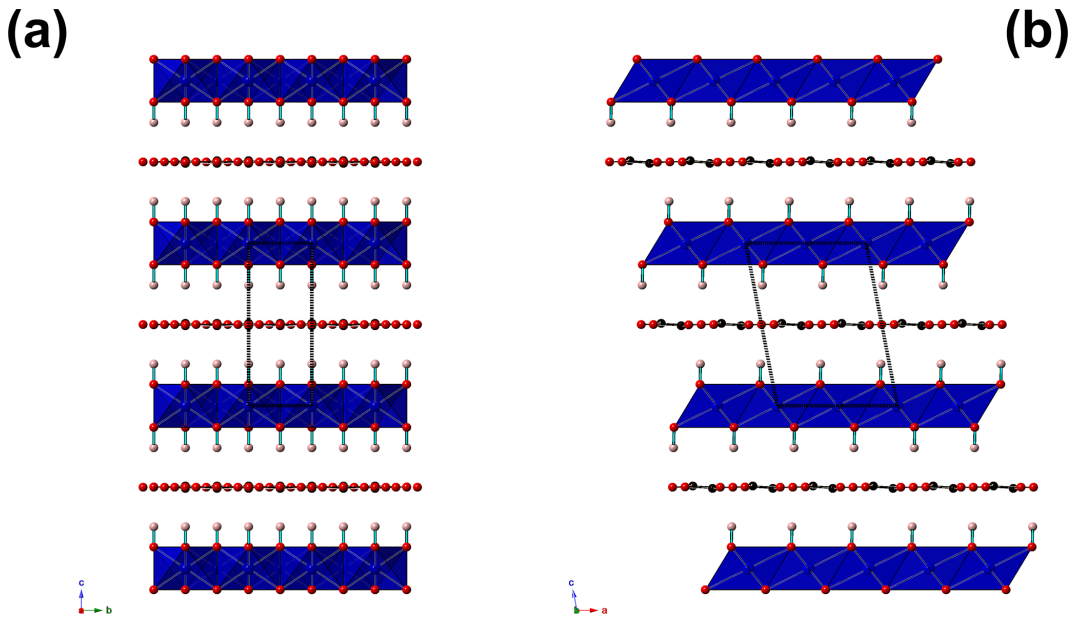

Figure 4. Projection of the crystal structure of marioantofilliite along a **(a)** and b **(b)**. The distorted brucite-like layer is formed by (Cu,Al)-centred octahedra (blue). Red and pink circles are O and H atoms, respectively. O–H bonds are drawn as thick light-blue lines. C atoms are shown in black, with C–O bonds shown as thick black lines. The unit cell is shown as dashed black lines.

7.3 Anion coordination and possible H bonds

Oxygen atoms at the O(1) site, belonging to the distorted brucite-like layers, are bonded to three (Cu,Al) atoms hosted at $M(1)$. Two bonds are short (1.94 Å), whereas the third is longer (2.23 Å). The resulting bond-valence sum is 1.17 v.u. The coordination of this O atom is completed by an H atom. The distance H–O was restrained and refined to 0.94(2) Å. After correcting for the H bond, the bond-valence sum at O(1) is 0.99 or 1.01 v.u., in accord with the different H bonds with O(1i) or O(2i) in which it is involved.

The O atoms in the interlayer are hosted at partially occupied positions, O(1i) and O(2i). The former has site occupancy 0.34(3) and can belong to a CO_3 group or to an H_2O group. In the first case, it is at 1.28(2) Å from C atoms and forms O(1i)–O(2i) distances of $\sim$ 2.4 Å, slightly longer than an ideal value of $\sim$ 2.2 Å. The O(2i) site has partial occupancy 0.193(9) and belongs to CO_3 groups only. The edge O(2i)–O(2i) of the CO_3 group is shorter than the ideal one, i.e. $\sim$ 1.9 Å. The unrestrained geometry of the CO_3 group shows some deviations from the ideal value because of the uncertainty in the actual location of the atom positions. However, it can be considered satisfying and is in accord with the occurrence of CO_3 groups and H_2O groups in marioantofilliite. Moreover, the CO_3 group is prismatically coordinated by H atoms, as observed in other LDH phases (e.g. Zhitova et al., 2018). O(1i) and O(2i) are acceptors of H bonds from the (OH) groups belonging to the distorted brucite-like layers. These H bonds have a corresponding bond strength, calculated according to Ferraris and Ivaldi (1988), ranging between 0.16 and 0.18 v.u. Consequently, the O atoms at the O(1i) and O(2i) sites have a total bond-valence sum of 1.68 and 1.49 v.u. Such low values indicate that they are probably also acceptors of H bonds from H_2O groups located in the interlayer at the O(1i) site, when it is not bonded to C atoms. Indeed, H_2O groups can be acceptors of 0.34 v.u. from two (OH) groups belonging to different brucite-like layers, and such a bond-valence will be redistributed to O atoms of the CO_3 groups. Other short O$\cdots$O distances (e.g. O(1i)–O(2i) = 0.76(2) Å; O(1i)–O(1i) = 1.16(5) Å) indicate the necessity of long-range order within the interlayer.

7.4 Structural formula

Considering site multiplicity, the formula of marioantofilliite obtained through the crystal structure refinement is $[(Cu_{0.613(18)}Al_{0.387(18)})(OH)_2](CO_3)_{0.194} \cdot 0.486H_2O$ ($Z = 2$). Recalculating this formula on the basis of (Cu + Al) = 6 apfu, it becomes (with rounding errors) $[(Cu_{3.72}Al_{2.28})(OH)_{12}](CO_3)_{1.10} \cdot 3.06H_2O$, in accord with the ideal formula of marioantofilliite $[Cu_4Al_2(OH)_{12}](CO_3) \cdot 3H_2O$ ($Z = 1/3$).

8 Relation to other species

8.1 Marioantofilliite in the framework of hydrotalcite-supergroup minerals

Marioantofilliite is the natural analogue of synthetic Cu–Al LDH phases described by several authors (e.g. Yamaoka et al., 1989; Britto and Kamath, 2009). The

Table 7. Natural known Cu–Al oxysalts.

Mineral	Chemical formula	Cu : (Cu + Al)	a (Å)	b (Å)	c (Å)	α (°)	β (°)	γ (°)	s.g.	Ref.
Aubertite group										
Aubertite	$CuAl(SO_4)_2Cl{\cdot}14H_2O$	0.50	6.29	13.24	6.28	91.9	94.7	82.4	$P\bar{1}$	[1]
Chalcoalumite group										
Chalcoalumite	$CuAl_4(SO_4)(OH)_{12} \cdot 3H_2O$	0.20	10.23	8.93	17.10	90	95.8	90	$P2_1/n$	[2]
Chalcophyllite group										
Barrotite	$Cu_9Al(HSiO_4)_2[(SO_4)(HAsO_4)_{0.5}](OH)_{12} \cdot 8H_2O$	0.90	10.65	10.65	21.95	90	90	120	$P3_1$ or $P3_2$	[3]
Chalcophyllite	$Cu_{18}Al_2(AsO_4)_4(SO_4)_3(OH)_{24} \cdot 36H_2O$	0.90	10.76	10.76	28.68	90	90	120	$R\bar{3}$	[4]
Tiberiobardiite	$Cu_9Al[SiO_3(OH)]_2(OH)_{12}(H_2O)_6(SO_4)_{1.5} \cdot 10H_2O$	0.90	10.69	10.69	28.32	90	90	120	$R\bar{3}$	[5]
Chenevixite group										
Luetheite	$Cu_2Al_2(AsO_4)_2(OH)_4$	0.50	14.74	5.09	5.60	90	101.8	90	$P2_1/m$	[6]
Cyanotrichite group										
Camérolaite	$Cu_6Al_3(OH)_{18}(H_2O)_2[Sb(OH)_6](SO_4)$	0.67	6.33	2.91	10.73	93.8	96.3	79.0	$P1$	[7]
Carbonatecyanotrichite	$Cu_4Al_2(CO_3,SO_4)(OH)_{12} \cdot 2H_2O$	0.67	10.15	2.83	12.55	90	98.5	90	Unknown	[8]
Cyanotrichite	$Cu_4Al_2(SO_4)(OH)_{12} \cdot 2H_2O$	0.67	12.62	2.90	10.15	90	92.2	90	$C2/m$	[9]
Khaidarkanite	$Cu_4Al_3(OH)_{14}F_3 \cdot 2H_2O$	0.57	12.35	2.91	10.37	90	97.9	90	$C2/m$	[10]
Hydrotalcite supergroup										
Cualstibite-1M	$Cu_2Al(OH)_6[Sb(OH)_6]$	0.67	9.94	8.89	5.49	90	102.9	90	$P2_1/c$	[11]
Cualstibite-1T	$Cu_2Al(OH)_6[Sb(OH)_6]$	0.67	9.15	9.15	9.74	90	90	120	$P3$	[12]
Hydrowoodwardite	$(Cu_{1-x}Al_x)(OH)_2(SO_4)_{x/2} \cdot nH_2O$	~ 1.00	3.07	3.07	31.9	90	90	120	$R\bar{3}m$	[13]
Marioantofilliite	$[Cu_4Al_2(OH)_{12}](CO_3){\cdot}\ 3H_2O$	0.67	5.59	2.94	7.68	90	101.0	90	$C2/m$	[14]
Woodwardite	$(Cu_{1-x}Al_x)(OH)_2(SO_4)_{x/2} \cdot nH_2O$				Not available					[15]
Liroconite group										
Liroconite	$Cu_2Al(AsO_4)(OH)_4 \cdot 4H_2O$	0.67	12.64	7.57	9.88	90	91.3	90	$I2/c$	[16]
Mixite group										
Goudeyite	$AlCu_6(AsO_4)_3(OH)_6 \cdot 3H_2O$	0.86	13.47	13.47	5.90	90	90	120	$P6_3/m$ or $P6_3$	[17]
Other oxysalts										
Ceruleite	$CuAl_4(AsO_4)_2(OH)_8 \cdot 4H_2O$	0.20	7.20	11.34	9.86	90	105.6	90	$P2_1/n$	[18]
Chrysocolla	$Cu_{2-x}Al_x(H_{2-x}Si_2O_5)(OH)_4 \cdot nH_2O$, $x < 1$	~ 0.9	4.9–6.2	8.9	6.4–8.6					[19]
Forêtite	$Cu_2Al_2(AsO_4)(OH,O,H_2O)_6$	0.50	6.97	7.68	8.59	82.0	71.7	102.7	$P\bar{1}$	[20]
Grandviewite	$Cu_3Al_2(SO_4)(OH)_{10}{\cdot}H_2O$	0.60	5.71	10.14	10.98	72.2	82.8	86.1	$P\bar{1}$	[21]
Sieleckiite	$Cu_3Al_4(PO_4)_2(OH)_{12} \cdot 2H_2O$	0.43	11.71	6.92	9.83	90	92.9	90	$C2/m$	[22]
Urusovite	$CuAl(AsO_4)O$	0.50	7.34	10.26	5.60	90	99.8	90	$P2_1/c$	[23]
Zapatalite	$Cu_3Al_4(PO_4)_3(OH)_9 \cdot 4H_2O$	0.50	15.22	15.22	11.52	90	90	90	Unknown	[24]
Spangolite group										
Llantenesite	$Cu_6Al[SeO_4](OH)_{12}Cl{\cdot}3H_2O$	0.86	8.26	8.26	14.60	90	90	120	$P31c$	[25]
Spangolite	$Cu_6Al(SO_4)(OH)_{12}Cl{\cdot}3H_2O$	0.86	8.25	8.25	14.35	90	90	120	$P31c$	[26]
Turquoise group										
Turquoise	$CuAl_6(PO_4)_4(OH)_8 \cdot 4H_2O$	0.14	7.41	7.63	9.90	68.4	69.6	65.0	$P\bar{1}$	[27]

s.g.: space group; [1] Cesbron et al. (1979); [2] Hawthorne and Cooper (2013); [3] Sarp et al. (2014); [4] Sabelli (1980); [5] Biagioni et al. (2018); [6] Williams (1977); [7] Mills et al. (2014); [8] Hager et al. (2009); [9] Mills et al. (2015); [10] Chukanov et al. (1999); [11] Kolitsch et al. (2013); [12] Bonaccorsi et al. (2007); [13] Witzke (1999); [14] this work; [15] Raade et al. (1985); [16] Plumhoff et al. (2020); [17] Wise (1978); [18] Mills et al. (2018); [19] Van Oosterwyck-Gastuche (1970); [20] Mills et al. (2012b); [21] Sejkora et al. (2022); [22] Elliott (2017); [23] Krivovichev et al. (2000); [24] Williams (1972); [25] Lengauer et al. (2019); [26] Hawthorne et al. (1993); [27] Kolitsch and Giester (2000).

relationship with hydrotalcite-supergroup minerals is also supported by the micro-Raman spectrum, which is very similar to those of other members of this supergroup, e.g. quintinite, $[Mg_4Al_2(OH)_{12}](CO_3){\cdot}\ 3H_2O$; caresite, $[Fe_4Al_2(OH)_{12}](CO_3){\cdot}\ 3H_2O$; and charmarite, $[Mn_4Al_2(OH)_{12}](CO_3){\cdot}\ 3H_2O$ (Theiss et al., 2015; Zhitova et al., 2024). As discussed above, in accordance with Zhitova et al. (2016), the basal spacing of ~ 7.6 Å suggests that marioantofilliite is close to members of the quintinite group. It is worth noting that deviations from the ideal $M^{2+} : M^{3+}$ ratio of 2 : 1 are known in the quintinite group. For instance, Zhitova et al. (2016) reported ratios of up to 2.38, not far from the value observed in marioantofilliite (~ 2.45).

Marioantofilliite is atypical for M^{2+}–M^{3+} disordered LDH phases. Indeed, the lowering of symmetry from trigonal/hexagonal to monoclinic is usually the result of cation ordering, whereas in marioantofilliite, Cu and Al are disordered at the $M(1)$ site. Thus, the monoclinic symmetry could be due to the octahedral distortion related to the Jahn–Teller effect of Cu^{2+}, which displays a (4 + 2) coordination, with a difference between the longest and the shortest bond distances of 0.29 Å. In quintinite polytypes, bond distances are more regular. For instance, in quintinite-2T, the Mg–O distances range between 2.054 and 2.076 Å, whereas Al atoms show six distances at 1.926 Å (Zhitova et al., 2018). As previously reported by Intissar et al. (2015), an increase in the

Cu content in the $(Mg_{4-x}Cu_x)Al_2(OH)_{12}(CO_3)\cdot nH_2O$ series results in a gradual transition, between $x = 2.6$ and 3.4, from the rhombohedral Mg_4Al_2 LDH structure to the monoclinic Cu_4Al_2 LDH one. This may be further evidence of the role played by Cu in favouring the lowering of symmetry.

8.2 Relationships between marioantofilliite and other Cu–Al oxysalts

Table 7 compares marioantofilliite with currently known Cu–Al oxysalts. Marioantofilliite is chemically similar, but very probably not identical, to carbonatecyanotrichite. Indeed, even if the chemical formula of this latter mineral is given as $Cu_4Al_2(CO_3)(OH)_{12}\cdot 2H_2O$, the possible occurrence of (SO_4) groups cannot be discarded (e.g. Hager et al., 2009). Moreover, the X-ray powder diffraction pattern of carbonatecyanotrichite is different from that of marioantofilliite (see, for instance, Hager et al., 2009) and suggests that the former is related to khaidarkanite, whose crystal structure, solved by Rastsvetaeva et al. (1997), is topologically different from the structures of hydrotalcite-supergroup compounds. Indeed, on the basis of this possible relationship, Hager et al. (2009) hypothesized that the formula of carbonatecyanotrichite could be written as $[Cu_4Al_2(OH)_{12}][Al(OH)_3]_{0.49}(CO_3)_{0.7}(SO_4)_{0.3}\cdot 2H_2O$. The $[Cu_4Al_2(OH)_{12}]^{2+}$ module occurring in the carbonatecyanotrichite would be represented by ribbons that are topologically different from the $[Cu_4Al_2(OH)_{12}]$ brucite-like layers of marioantofilliite.

9 Conclusion

The discovery of marioantofilliite has implications for both materials science and Earth sciences. Indeed, it is the natural analogue of some synthetic Cu–Al LDH phases actively studied for their catalytic and anion exchange properties (e.g. Busetto et al., 1984; Yamaoka et al., 1989; Kiani et al., 2022). The solution and description of its crystal structure using single-crystal X-ray diffraction can thus be a meaningful step in the knowledge of this technologically significant material.

Moreover, marioantofilliite is the second new mineral species described from ophiolite-hosted Cu ore deposits of the northern Apennines, and its discovery confirms the necessity of improving our knowledge of the supergene mineral assemblages related to the alteration of primary Cu–Fe ores. This would have implications not only for mineral systematics, due to the possible identification of rare or even new mineral species, but also for a better understanding of the fate of several elements (e.g. Cu, Fe) in the alteration zone of these ore deposits. It is also an additional case of CO_2 sequestration by supergene mineral assemblages hosted in (meta)ophiolites. In such environments, some case studies involving the precipitation of Mg carbonates, among which LDH phases are included, are known, e.g. Montecastelli Pisano, Tuscany (Boschi et al., 2017), and Monte Ramazzo (Artini, 1922; Lincio, 1930). It is worth noting that in the latter locality the interaction between low-T CO_2-rich fluids and ophiolite-hosted ore minerals favoured the crystallization of several rare or even endemic carbonate species, also containing transition elements (Cu, Co) like ramazzoite and perchiazziite (Kampf et al., 2018; Barbaro et al., 2024). This suggests the opportunity to collect further data on the supergene mineral assemblages related to ophiolite-hosted ore deposits.

Data availability. The crystallographic information file and the X-ray powder diffraction data of marioantofilliite are available in the Supplement.

Supplement. The supplement related to this article is available online at https://doi.org/10.5194/ejm-37-733-2025-supplement.

Author contributions. CB carried out the X-ray diffraction study. JS and ZD performed thermogravimetric and evolved-gas analysis, as well as electron microprobe analysis. JS and DM collected micro-Raman spectra. NP examined X-ray powder diffraction patterns. EM performed the transmission electron microscopy study. RS measured optical properties. CB, NP, and DB critically examined the data. CB wrote the paper, with inputs from the other authors.

Competing interests. At least one of the (co-)authors is a member of the editorial board of the *European Journal of Mineralogy*. The peer-review process was guided by an independent editor, and the authors also have no other competing interests to declare.

Disclaimer. Publisher's note: Copernicus Publications remains neutral with regard to jurisdictional claims made in the text, published maps, institutional affiliations, or any other geographical representation in this paper. While Copernicus Publications makes every effort to include appropriate place names, the final responsibility lies with the authors.

Acknowledgements. Sebastiano Di Lisi is acknowledged for providing us with the specimen of marioantofilliite used for this mineralogical investigation. The comments of Elena Zhitova and Sergey Britvin improved the original manuscript.

Financial support. This research has been supported by the Ministry of Culture of the Czech Republic (long-term project DKRVO 2024-2028/1.II.b; National Museum, 00023272) through funding for Jiří Sejkora and Zdeněk Dolníček.

Review statement. This paper was edited by Sergey Krivovichev and reviewed by Elena Zhitova and Sergey Britvin.

References

Alt, J., Crispini, L., Gaggero, L., Levine, D., Lavagnino, G., Shanks, P., and Gulbransen, C.: Normal faulting and evolution of fluid discharge in a Jurassic seafloor ultramafic-hosted hydrothermal system, Geology, 46, 523–526, 2018.

Antofilli, M.: Le zeoliti della Liguria, Riv. Mineral. Ital., 6, 7–14, 1982.

Antofilli, M., Borgo, E., and Palenzona, A.: I nostri minerali, Geologia e mineralogia in Liguria, Sagep, Genova, 295 pp., 1983.

Artini, E.: Sulla Brugnatellite di Monte Ramazzo (Genova), Rend. R. Accad. Lincei, 31, 491–496, 1922.

Barbaro, A., Nestola, F., Kasatkin, A. V., Ardit, M., Rotiroti, N., Škoda, R., Agakhanov, A. A., Dalconi, M. C., and Castellaro, F.: Perchiazziite, $Co_2(CO_3)(OH)_2$, a new member of the rosasite-malachite group from the Monte Ramazzo mine, Italy, Can. J. Mineral. Petrol., 62, 369–378, 2024.

Bardi, T., Bazzoni, C., Bernocchi, M., Betti, C., Biagioni, C., D'Orazio, M., and Pagani, G.: Cretaio. La vecchia ricerca cuprifera presso Prata, Massa Marittima (GR), Riv. Mineral. Ital., 41, 104–118, 2017.

Bertolani, M. and Rivalenti, G.: Le mineralizzazioni metallifere della miniera di Montecatini Val di Cecina (Pisa), Boll. Soc. Geol. Ital., 92, 635–648, 1973.

Biagioni, C., Pasero, M., and Zaccarini, F.: Tiberiobardiite, $Cu_9Al_2(SiO_3OH)_2(OH)_{12}(H_2O)_6(SO_4)_{1.5}\bullet 10H_2O$, a new mineral related to chalcophyllite from the Cretaio Cu prospect, Massa Marittima, Grosseto (Tuscany, Italy): occurrence and crystal structure, Minerals, 8, 152, https://doi.org/10.3390/min8040152, 2018.

Bonaccorsi, E., Merlino, S., and Orlandi, P.: Zincalstibite, a new mineral, and cualstibite: Crystal chemical and structural relationships, Am. Mineral., 92, 198–203, 2007.

Bonatti, S. and Trevisan, L.: Notizie preliminari sul giacimento cuprifero di Reppia (Chiavari), Rend. Soc. Mineral. Ital., 1, 87–97, 1941.

Boschi, C., Dini, A., Baneschi, I., Bedini, F., Perchiazzi, N., and Cavallo, A.: Brucite-driven CO_2 uptake in serpentinized dunites (Ligurian Ophiolites, Montecastelli, Tuscany), Lithos, 288–289, 264–281, 2017.

Boulahbal, A. I., Santamaría, L., Azizi, A., Boutahala, M., Korili, S. A., and Gil, A.: Synthesis of Cu-Al layered double hydroxides from aluminum saline slags, Miner. Engin., 204, 108413, https://doi.org/10.1016/j.mineng.2023.108413, 2023.

Britto, S. and Kamath, P. V.: Thermal, solution and reductive decomposition of Cu–Al layered double hydroxides into oxide products, J. Solid St. Chem., 182, 1193–1199, 2009.

Bruker AXS Inc.: APEX4. Bruker Advanced X-ray Solutions, Madison, Wisconsin, USA, 2022.

Burns, P. C. and Hawthorne, F. C.: Static and dynamic Jahn-Teller effects in Cu^{2+}-oxysalt minerals, Can. Mineral., 34, 1089–1105, 1996.

Busetto, C., Del Piero, G., Manara, G., Trifirò, F., and Vaccari, A.: Catalysts for low-temperature methanol synthesis. Preparation of Cu–Zn–Al mixed oxides via hydrotalcite-like precursors, J. Catalysis, 85, 260–266, 1984.

Camarda, S., Muzio, C., Passarino, G., and Sanguineti, G.: Reppia, Ne, Val Graveglia, Genova. Minerali secondari di un giacimento ferroso cuprifero, Riv. Mineral. Ital., 37, 176–185, 2013.

Čejka, J., Sejkora, J., Jebavá, I., Xi, Y., Couperthwaite, S., and Frost, R. L.: A Raman spectroscopic study of the basic carbonate mineral callaghanite $Cu_2Mg_2(CO_3)(OH)_6 \cdot 2H_2O$, Spectrochim. Acta Part A, 108, 171–176, 2013.

Cesbron, F., Ginderow, D., Sichère, M. C., and Vachey, H.: L'aubertite, un noveau chloro-sulfate hydraté de cuivre et d'aluminium, Bull. Minéral., 102, 348–350, 1979.

Chukanov, N. V., Karpenko, V. Y., Rastsvetaeva, R. K., Zadov, A. E., and Kuz'mina, O.V.: Khaidarkanite, $Cu_4Al_3(OH)_{14}F_3 \cdot 2H_2O$, new mineral from Khaidarkan deposit, Kyrgyzstan, Zap. Vseros. Mineral. Obsh., 128, 58–63, 1999 (in Russian).

Coelho, A. A.: TOPAS and TOPAS-Academic: an optimization program integrating computer algebra and crystallographic objects written in C++, J. Appl. Crystallogr., 51, 210–218, 2018.

Coombs, D. S., Alberti, A., Armbruster, T., Artioli, G., Colella, C., Galli, E., Grice, J. D., Liebau, F., Mandarino, J. A., Minato, H., Nickel, E. H., Passaglia, E., Peacor, D. R., Quartieri, S., Rinaldi, R., Sheppard, R. A., Tillmanns, E., and Vezzalini, G.: Recommended nomenclature for zeolite minerals: report of the Subcommittee on zeolites of the International Mineralogical Association, Commission on New Minerals and Mineral Names, Can. Mineral., 35, 1571–1606, 1997.

D'Achiardi, A.: Mineralogia della Toscana. Vol. II, Tipografia Nistri, Pisa, 404 pp., 1873.

Dini, A., Rielli, A., Di Giuseppe, P., Ruggieri, G., and Boschi, C.: The ophiolite-hosted Cu-Zn VMS deposits of Tuscany (Italy), Minerals, 14, 273, https://doi.org/10.3390/min14030273, 2024.

Elliott, P.: Refinement of the crystal structure of sieleckiite and revision of its symmetry, Mineral. Mag., 81, 917–922, 2017.

Ferrario, A. and Garuti, G.: Copper deposits in the basal breccias and volcano-sedimentary sequences of the Eastern Ligurian Ophiolites (Italy), Miner. Dep., 15, 291–303, 1980.

Ferraris, G. and Ivaldi, G.: Bond valence vs bond length in O···O hydrogen bonds, Acta Crystallogr., B44, 341–344, 1988.

Franzini, M. and Perchiazzi, N.: Portite discredited = natrolite and new data on "schneiderite" (= laumontite), Eur. J. Mineral., 6, 351–353, 1994.

Frost, R.L., Soisnard, A., Voyer, N., Palmer, S. J., and Martens, W. N.: Thermo-Raman spectroscopy of selected layered double hydroxides of formula $Cu_6Al_2(OH)_{16}CO_3$ and $Zn_6Al_2(OH)_{16}CO_3$, J. Raman Spectr., 40, 645–649, 2009.

Gagné, O. C. and Hawthorne, F. C.: Comprehensive derivation of bond-valence parameters for ion pairs involving oxygen, Acta Crystallogr., B71, 562–578, 2015.

Garuti, G., Bartoli, O., Scacchetti, M., and Zaccarini, F.: Geological setting and structural styles of Volcanic Massive Sulfide deposits in the northern Apennines (Italy): evidence for seafloor and subseafloor hydrothermal activity in unconventional ophiolites of the Mesozoic Tethys, Bol. Soc. Geol. Mex., 60, 121–145, 2008.

Gemmi, M., Mugnaioli, E., Gorelik, T. E., Kolb, U., Palatinus, L., Boullay, P., Hovmöller, S., and Abrahams, J. P.: 3D Electron Diffraction: the nanocrystallography revolution, ACS Cent. Sci., 5, 1315–1329, 2019.

Gramaccioli, C. M., Griffin, W. L., and Mottana, A.: Tiragalloite, $Mn_4[AsSi_3O_{12}(OH)]$, a new mineral and the first example of arsenatotrisilicate, Am. Mineral., 65, 947–952, 1980.

Hager, S. L., Leverett, P., and Williams, P. A.: Possible structural and chemical relationships in the cyanotrichite group, Can. Mineral., 47, 635–648, 2009.

Hawthorne, F. C. and Cooper, M. A.: The crystal structure of chalcoalumite: mechanisms of Jahn-Teller-driven distortion in $^{[6]}Cu^{2+}$-containing oxysalts, Mineral. Mag., 77, 2901–2912, 2013.

Hawthorne, F. C., Kimata, M., and Eby, R. K.: The crystal structure of spangolite, a complex copper sulfate sheet mineral, Am. Mineral., 78, 649–652, 1993.

Intissar, M., Seron, A., Giovannelli, F., Autret, C., Motelica-Heino, M., and Delorme, F.: Effect of copper content on the synthesis and properties of $(Mg_{4-x}Cu_x)Al_2OH_{12}CO_3$, nH_2O layered double hydroxides, J. Mat. Sci., 50, 1427–1434, 2015.

Kampf, A. R., Rossman, G. R., Ma, C., Belmonte, D., Biagioni, C., Castellaro, F., and Chiappino, L.: Ramazzoite, $[Mg_8Cu_{12}(PO_4)(CO_3)_4(OH)_{24}(H_2O)_{20}][(H_{0.33}SO_4)_3(H_2O)_{36}]$, the first mineral with a polyoxometalate cation, Eur. J. Mineral., 30, 827–834, 2018.

Kiani, M., Bagherzadeh, M., Ghadiri, A. M., Makvandi, P., and Rabiee, N.: Multifunctional green synthesized Cu–Al layered double hydroxide (LDH) nanoparticles: anti-cancer and antibacterial activities, Sci. Rep., 12, 9461, https://doi.org/10.1038/s41598-022-13431-7, 2022.

Kolitsch, U. and Giester, G.: The crystal structure of faustite and its copper analogue turquoise, Mineral. Mag., 64, 905–913, 2000.

Kolitsch, U., Giester, G., and Pippinger, T.: The crystal structure of cualstibite-1*M* (formerly cyanophyllite), its revised chemical formula and its relation to cualstibite-1*T*, Mineral. Petrol., 107, 171–178, 2013.

Kraus, W. and Nolze, G.: PowderCell – a program for the representation and manipulation of crystal structures and calculation of the resulting X-ray powder patterns, J. Appl. Crystallogr., 29, 301–303, 1996.

Krivovichev, S. V., Molchanov, A. V., and Filatov, S. K.: Crystal structure of urusovite, $Cu[AlAsO_5]$: a new type of a tetrahedral aluminoarsenate polyanion, Crystallogr. Rep., 45, 723–727, 2000.

Lengauer, C. L., Ende, M., Topa, D., Lira, R., and Paar, W. H.: Llantenesite, IMA 2018-111. CNMNC Newsletter No. 47, February 2019, page 145, Mineral. Mag., 83, 143–147, 2019.

Lincio, A.: Sull'artinite di Monte Ramazzo (Liguria), Rend. R. Accad. Lincei, 11, 420–424, 1930.

Lucchetti, G., Massa, B., and Penco, A. M.: Strontian heulandite from Campegli (Eastern Ligurian ophiolites, Italy), N. Jahr. Miner. Monat., 1982, 541–550, 1982.

Majzlan, J., Števko, M., Chovan, M., Luptáková, J., Milovská, S., Milovský, R., Jeleň,S., Sýkorová, M., Pollok, K., Göttlicher, J., and Kupka, D.: Mineralogy and geochemistry of the copper-dominated neutral mine drainage at the Cu deposit L'ubietová-Podlipa (Slovakia), Appl. Geochem., 92, 59–70, 2018.

Mandarino, J. A.: The Gladstone-Dale relationship. Part IV. The compatibility concept and some application, Can. Mineral., 19, 441–450, 1981.

Mills, S. J., Christy, A. G., Génin, J.-M. R., Kameda, T., and Colombo, F.: Nomenclature of the hydrotalcite supergroup: natural layered double hydroxides, Mineral. Mag., 76, 1289–1336, 2012a.

Mills, S. J., Kampf, A. R., McDonald, A. M., Favreau, G., and Chiappero, P. J.: Forêtite, a new secondary arsenate mineral from the Cap Garonne mine, France, Mineral. Mag., 76, 769–775, 2012b.

Mills, S. J., Christy, A. G., Schnyder, C., Favreau, G., and Price, J. R.: The crystal structure of camerolaite and structural variation in the cyanotrichite family of merotypes, Mineral. Mag., 78, 1527–1552, 2014.

Mills, S. J., Christy, A. G., Colombo, F., and Price, J. R.: The crystal structure of cyanotrichite, Mineral. Mag., 79, 321–335, 2015.

Mills, S. J., Christy, A. G., and Favreau, G.: The crystal structure of ceruleite, $CuAl_4[AsO_4]_2(OH)_8(H_2O)_4$, from Cap Garonne, France, Mineral. Mag., 82, 181–187, 2018.

O'Neill, H. S. C., James, M., Dollase, W. A., and Redfern, S. A.: Temperature dependence of the cation distribution in $CuAl_2O_4$ spinel, Eur. J. Mineral., 17, 581–586, 2005.

Pérez-Ramírez, J., Mul, G., and Moulijn, J. A.: In situ Fourier transform infrared and laser Raman spectroscopic study of the thermal decomposition of Co–Al and Ni–Al hydrotalcites, Vib. Spectr., 27, 75–88, 2001.

Plumhoff, A. M., Plášil, J., Dachs, E., Benisek, A., Sejkora, J., Števko, M., Rumsey, M. S., and Majzlan, J.: Thermodynamic properties, crystal structure and phase relations of pushcharovskite $[Cu(AsO_3OH)(H_2O)\cdot 0.5H_2O]$, geminite $[Cu(AsO_3OH)(H_2O)]$ and liroconite $[Cu_2Al(AsO_4)(OH)_4\cdot 4H_2O]$, Eur. J. Mineral., 32, 285–304, https://doi.org/10.5194/ejm-32-285-2020, 2020.

Pouchou, J. L. and Pichoir, F.: "PAP" ($\varphi\rho$Z) procedure for improved quantitative microanalysis, 104–106, in: Microbeam Analysis, edited by: Armstrong, J. T., San Francisco Press, San Francisco, 1985.

Raade, G., Elliott, C. J., and Din, V. K.: New data on glaucocerinite, Mineral. Mag., 49, 583–590, 1985.

Rastsvetaeva, R. K., Chukanov, N. V., and Karpenko, V. Y.: Crystal structure of a new native compound $Cu_4Al_3(OH)_{14}F_3(H_2O)_2$, Dokl. Chem., 353, 45–48, 1997.

Sabelli, C.: The crystal structure of chalcophyllite, Z. Kristallogr., 151, 129–140, 1980.

Sarp, H., Černý, R., Pushcharovsky, D. Y., Schouwink, P., Teyssier, J., Williams, P. A., Babalik, H., and Mari, G.: La barrotite, $Cu_9Al(HSiO_4)_2[(SO_4)(HAsO_4)_{0.5}](OH)_{12}\cdot 8H_2O$, un noveau minéral de la mine de Roua (Alpes-Maritimes, France), Riv. Sci., 98, 3–22, 2014.

Sejkora, J., Steciuk, G., Marquez-Zavalia, M.F., Plášil, J., and Dolníček, Z.: Grandviewite redefinition, new formula $Cu_3Al_2(SO_4)(OH)_{10}\cdot H_2O$, and crystal-structure determination, Mineral. Mag., 86, 730–742, 2022.

Sheldrick, G. M.: SHELXT – Integrated space-group and crystal-structure determination, Acta Crystallogr., A71, 3–8, 2015a.

Sheldrick, G. M.: Crystal structure refinement with SHELXL, Acta Crystallogr., C71, 3–8, 2015b.

Theiss, F., López, A., Frost, R. L., and Scholz, R.: Spectroscopic characterisation of the LDH mineral quintinite $Mg_4Al_2(OH)_{12}CO_3\cdot 3H_2O$, Spectrochim. Acta Part A, 150, 758–764, 2015.

Van Oosterwyck-Gastuche, M. C.: La structure de la chrysocolle, Compt. R. Hebd. séanc. Acad. Sci., 271, 1837–1840, 1970.

Vieira, A. C., Moreira, R. L., and Dias, A.: Raman scattering and Fourier transform infrared spectroscopy of $Me_6Al_2(OH)_{16}Cl_2\cdot 4H_2O$ (Me = Mg, Ni, Zn, Co, and Mn) and

$Ca_2Al(OH)_6Cl{\cdot}2H_2O$ hydrotalcites, J. Phys. Chem. C, 113, 13358–13368, 2009.

Williams, S. A.: Zapatalite, a new mineral from Sonora, Mexico, Mineral. Mag., 38, 541–544, 1972.

Williams, S. A.: Luetheite, $Cu_2Al_2(AsO_4)_2(OH)_4.H_2O$, a new mineral from Arizona, compared with chenevixite, Mineral. Mag., 41, 27–32, 1977.

Wilson, A. J. C. (Ed.): International Tables for Crystallography, Volume C: Mathematical, physical and chemical tables, Kluwer Academic, Dordrecht, NL, 1992.

Wise, W. S.: Parnauite and goudeyite, two new copper arsenate minerals from the Majuba Hill mine, Pershing County, Nevada, Am. Mineral., 63, 704–708, 1978.

Witzke, T.: Hydrowoodwardite, a new mineral of the hydrotalcite group from Königswalde near Annaberg, Saxony/Germany and other localities, N. Jahr. Miner. Monat., 1999, 75–86, 1999.

Wright, F. E.: Computation of the optic axial angle from the three principal refractive indices, Am. Mineral., 36, 543–556, 1951.

Yamaoka, T., Abe, M., and Tsuji, M.: Synthesis of Cu-Al hydrotalcite like compound and its ion exchange property, Mat. Res. Bull., 24, 1183–1199, 1989.

Zhitova, E. S., Krivovichev, S. V., Pekov, I. V., Yakovenchuk, V. N., and Pakhomovsky, Y. A.: Correlation between the *d*-value and the $M^{2+}:M^{3+}$ cation ratio in Mg–Al–CO_3 layered double hydroxides, Appl. Clay Sci., 130, 2–11, 2016.

Zhitova, E. S., Krivovichev, S. V., Yakovenchuk, V. N., Ivanyuk, G. Y., Pakhomovsky, Y. A., and Mikhailova, J. A.: Crystal chemistry of natural layered double hydroxides: 4. Crystal structure and evolution of structural complexity of quintinite polytypes from the Kovdor alkaline-ultrabasic massif, Kola peninsula, Russia, Mineral. Mag., 82, 329–346, 2018.

Zhitova, E. S., Zolotarev, A. A., Kasatkin, A. V., Sheveleva, R. M., Krivovichev, S. V., Pekov, I. V., and Bocharov, V. N.: The crystal structure of charmarite – the first case of a 11×11 Å superstructure mesh in layered double hydroxides, Mineral. Mag., 88, 244–254, 2024.